THE JOURNAL OF BIOLOGICAL CHEMISTRY VOL. 283, NO. 37, pp. 25340–25347, September 12, 2008

Carbon Dioxide Transport through Membranes*

Received for publication, January 4, 2008, and in revised form, June 27, 2008 Published, JBC Papers in Press, July 9, 2008, DOI 10.1074/jbc.M800096200

Andreas Missner[‡], Philipp Kügler[§¶], Sapar M. Saparov[‡], Klaus Sommer[‡], John C. Mathai[‖], Mark L. Zeidel[‖], and Peter Pohl[‡1]

From the [‡]Institut für Biophysik and [§]Institut für Industriemathematik, Johannes Kepler Universität, Linz A-4040, Austria, [¶]Johan Radon Institute for Computational and Applied Mathematics, Austrian Academy of Sciences, Linz A-4040, Austria, and [‖]Beth Israel Deaconess Medical Center and Harvard Medical School, Boston, Massachusetts 02215

Several membrane channels, like aquaporin-1 (AQP1) and the RhAG protein of the rhesus complex, were hypothesized to be of physiological relevance for CO_2 transport. However, the underlying assumption that the lipid matrix imposes a significant barrier to CO_2 diffusion was never confirmed experimentally. Here we have monitored transmembrane CO_2 flux (J_{CO2}) by imposing a CO_2 concentration gradient across planar lipid bilayers and detecting the resulting small pH shift in the immediate membrane vicinity. An analytical model, which accounts for the presence of both carbonic anhydrase and buffer molecules, was fitted to the experimental pH profiles using inverse problems techniques. At pH 7.4, the model revealed that J_{CO2} was entirely rate-limited by near-membrane unstirred layers (USL), which act as diffusional barriers in series with the membrane. Membrane tightening by sphingomyelin and cholesterol did not alter J_{CO2} confirming that membrane resistance was comparatively small. In contrast, a pH-induced shift of the CO_2 hydration-dehydration equilibrium resulted in a relative membrane contribution of about 15% to the total resistance (pH 9.6). Under these conditions, a membrane CO_2 permeability (3.2 ± 1.6 cm/s) was estimated. It indicates that cellular CO_2 uptake (pH 7.4) is always USL-limited, because the USL size always exceeds 1 μm. Consequently, facilitation of CO_2 transport by AQP1, RhAG, or any other protein is highly unlikely. The conclusion was confirmed by the observation that CO_2 permeability of epithelial cell monolayers was always the same whether AQP1 was overexpressed in both the apical and basolateral membranes or not.

The widely accepted model that gases like NH_3, CO_2, and O_2 pass biological membranes by diffusion through the lipid matrix has been recently called into question. For example, the membrane protein channels AmtB and aquaporin-8 have been identified to transport NH_3 (1, 2). Protein channels such as the human aquaporin-1, the plant aquaporin NtAQP1, and the RhAG protein of the rhesus complex were reported to provide a pathway for CO_2 transport (3–5). The similarity in the findings for NH_3 and CO_2 is very surprising because Overtone's rule predicts that their permeabilities, P_M, across the lipid phase of biological membranes differ 750-fold. The number was calculated assuming that NH_3 and CO_2 have comparable membrane diffusivities and that neither one of them belongs to those extremely rare exceptions from Overtone's rule (6, 7) so that the proportionality between P_M and the biphasic partition coefficient (water/organic solvent) applies as shown in Equation 1,

$$P_{M,CO_2} = P_{M,NH_3} K_{CO_2}/K_{NH_3} = 12\ \text{cms}^{-1} \qquad \text{(Eq. 1)}$$

where $K_{CO2} \sim 1.5$ (8), $K_{NH3} \sim 0.002$ (6), and $P_{M,NH3} = 0.016$ cm/s (9).

A $P_{M,CO2}$ of 12 cm/s suggests that the lipid matrix of biological membranes cannot act as a barrier to CO_2 diffusion. In fact, a stagnant water layer adjacent to the membrane that has the same thickness (δ) as the membrane would generate the same resistance to CO_2 flow as is caused by the membrane itself. Because these so-called unstirred layers (USL)[2] are unavoidably present in the vicinity of all biological membranes (10) and because their size always exceeds membrane thickness by several orders of magnitude, the contribution of membrane resistance to the overall resistance to CO_2 flow is expected to be negligibly small. Thus, lowering membrane resistance by insertion of CO_2 conducting channels seems to be of questionable physiological relevance. This is exactly what has been concluded from a study where red blood cell aquaporin-1 has been knocked out without any effect on $P_{M,CO2}$ (11). This view is further supported by molecular dynamics simulations of CO_2 transport through AQP1, which revealed that such a transport process would be physiologically meaningless in phospholipid membranes of common composition (12, 13).

In contrast, Endeward *et al.* (3) reported that AQP1 accounts for over 50% of $P_{M,CO2}$ in normal red blood cells at physiological pH. Loss of Rh protein complex reduced $P_{M,CO2}$ from initially 0.15 to 0.07 cm/s (5). Because the $P_{M,CO2}$ of 0.07 cm/s is in sharp contrast to the predicted value of 12 cm/s, this study aims to elucidate whether CO_2 is an exception from Overtone's rule. In case of applicability of Overtone's rule to CO_2 transport, neither AQP1 nor Rh proteins would be able to facilitate CO_2 membrane diffusion.

EXPERIMENTAL PROCEDURES

Planar Lipid Membranes—Planar bilayer lipid membranes were formed from the following: (i) pure diphytanoyl-phosphatidylcholine (DPhPC), (ii) from a 3:2:1 mixture of choles-

* This work was supported, in whole or in part, by National Institutes of Health Grants DK43955 and DK048217 (to M. Z. L. and J. C. M.). This work was also supported by Austrian Science Fund FWF W1201-N13 (to P. P.). The costs of publication of this article were defrayed in part by the payment of page charges. This article must therefore be hereby marked "*advertisement*" in accordance with 18 U.S.C. Section 1734 solely to indicate this fact.

[1] To whom correspondence should be addressed: Altenbergerstr. 69, A-4040 Linz, Austria. Fax: 43-732-2468-9269; E-mail: peter.pohl@jku.at.

[2] The abbreviations used are: USL, unstirred layer; FITC, fluorescein isothiocyanate; MDCK, Madin-Darby canine kidney; PBS, phosphate-buffered saline; DPhPC, diphytanoyl-phosphatidylcholine; SM, sphingomyelin; AQP1, aquaporin-1; CA, carbonic anhydrase; hAQP1, human AQP1.

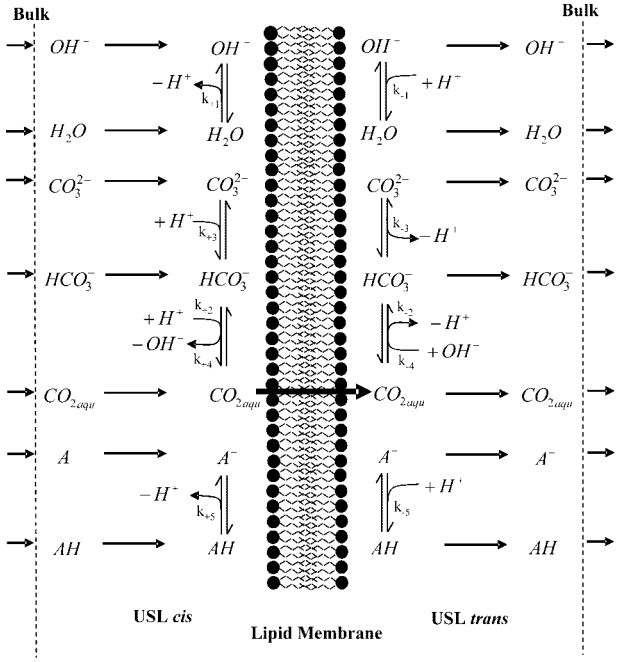

FIGURE 1. **The membrane system shows two USLs in the immediate vicinity of a lipid membrane.** Diffusion of CO_2 across a lipid bilayer includes several steps (from *left to right*). First the protonated and deprotonated forms of all participating molecules diffuse from the bulk across the *cis* USL to the membrane surface. Here HCO_3^- and CO_3^{2-} get protonated to form CO_2. The buffer AH provides an additional proton source. Following Overton's Rule uncharged CO_2 permeates the membrane and gets deprotonated on the other side. The buffering molecule A^- at the transmembrane surface now serves as proton sink. Finally the protonated and deprotonated forms of all species diffuse across the *trans* USL into the bulk.

terol, DPhPC, and egg sphingomyelin (SM, 84% palmitoyl-SM, 6% stearoyl-SM, 10% longer saturated acyl chain SM), or (iii) from a mixture that mimicked the lipid composition of the red cell plasma membrane. It was composed of egg phosphatidylcholine, egg phosphatidylethanolamine, brain phosphatidylserine, cholesterol, and SM (all Avanti Polar Lipids, Alabaster, AL) (14). The lipids were dissolved at 20 mg/ml in *n*-decane (15) and were spread across a 250–300-μm circular hole in a septum separating two aqueous compartments (each 1.4 ml) of a Teflon chamber. Bilayer capacitance and conductance were continuously monitored by a picoamperometer (model VA10, NPI Electronic GmbH, Tamm, Germany) connected via Ag/AgCl electrodes situated at both sides of the membrane. The aqueous salt solutions contained 66 mM NaCl (Merck). Depending on pH, they were either buffered with 30 mM HEPES (Fluka, Vienna, Austria) or 30 mM CAPSO (Sigma). After a stable planar membrane was formed $NaHCO_3$, Na_2CO_3, and carbonic anhydrase (Merck) were added to one or both sides of the membrane (see figure legends), and the chamber was covered with a Teflon lid. Magnetic stirrer bars continuously agitated the solutions.

Belonging to the class of weak acids, CO_2 transport across membranes includes several steps (Fig. 1) as follows: (*a*) the diffusion of HCO_3^- ($pK_{HCO3} = 6.1$) and CO_3^{2-} ($pK_{CO3} = 10$) to the planar membrane; (*b*) proton uptake; (*c*) diffusion of CO_2 through the bilayer; (*d*) dissociation, and (*e*) diffusion of HCO_3^- and CO_3^{2-} into the bulk. The buffering solution provides a proton source and a proton sink in the *cis* and *trans* USL, respectively. The chemical reactions were catalyzed by the presence of carbonic anhydrase (CA).

Cell Culture—Stably aquaporin-1-overexpressing Madin-Darby canine kidney (MDCK-AQP1) cells (16) and MDCK cells were cultured in Dulbecco's modified Eagle's medium supplemented with 110 mg/liter sodium pyruvate, 584 mg/liter L-glutamine, nonessential amino acids, 5% fetal calf serum, 20 mM HEPES, 0.1% $NaHCO_3$, and penicillin/streptomycin at 37 °C in 8.5% CO_2. The AQP1 expression vector includes the hygromycin B resistance gene. It allowed maintenance of selective pressure by adding 75 μg/ml hygromycin B to the AQP1-MDCK cell medium (16). For microelectrode measurements, the cells were seeded 1:1 onto semipermeable supports (Transwell, Costar) with a surface area of 0.33 cm^2 and cultured again until the electrical resistance reached >3 kΩ indicating a tight monolayer (usually after 3–4 days). All cell experiments were carried out in HBBS buffer (HBBS buffer = 118 mM NaCl, 4.6 mM KCl, 10 mM glucose, and 20 mM HEPES, pH 7.4) at 37 °C.

Immunoblots—Growing cells were harvested by scraping, washed twice in cold PBS, and lysed in RIPAII (500 mM NaCl; 50 mM Tris/HCl, pH 7.4; 0.1% SDS; 1% Nonidet P-40; 0.5% sodium deoxycholate; 0.05% NaN_3) for 30 min on ice. Lysates were sonified, and the cell debris was pelleted with 12,000 × *g*. The total protein concentration of the supernatant was determined by Bradford protein assay (Pierce). A quantity of 20 μg (plus one additional lane with 10 μg for the MDCK-AQP1 sample) of total protein per lane was separated by 12% SDS-PAGE on Mini Protean III (Bio-Rad) and transferred to polyvinylidene difluoride membranes (Pall). Membranes were blocked with 5% milk powder in 0.05% Tween/PBS, incubated with anti-hAQP1 antibody (Alpha Diagnostics), and the secondary antibodies Goat Anti-Rabbit IgG (Sigma) diluted in 1% milk powder/Tween/PBS. The target proteins on the membrane were detected by chemiluminescence using Bio-Rad Universal Hood II.

Immunofluorescence—Stably transfected MDCK-hAQP1 or nontransfected MDCK cells were seeded on coverslips and cultivated for at least 48 h before fixation. Cells were washed twice with PBS, fixed with 2% formaldehyde/PBS for 20 min at room temperature, washed twice with PBS, permeabilized with 0.2% Triton X-100/PBS for 20 min, and saturated with 0.2% fish gelatin. The cells were incubated with anti-hAQP1 antibody (10 μg/ml) followed by FITC-labeled secondary antibody. The coverslips were fixed on glass slides with DAKO fluorescent mounting medium. Cells were analyzed and pictured by a Zeiss confocal microscope (LSM 510).

Microelectrode Measurements—Because all kinetic measurements of CO_2 flux are compromised by USL effects, we monitored the accompanying pH changes in the steady state. A scanning pH-sensitive microelectrode was moved by a hydraulic microdrive manipulator (Narishige, Tokyo, Japan) within the stagnant water layer with a velocity of 2 μm/s toward or away from the membrane (17). Addition of CA did not affect the sensitivity of the electrode. Voltage recordings were performed every second with an electrometer (model 6514, Keithley Instruments), connected via an IEEE-488 interface to a personal computer. The electrodes were manufactured from borosilicate glass that was pulled to a tip size of 2–4 μm, silanized (bis(dimethylamino)dimethylsilane, Fluka), and filled with a

proton-sensitive mixture (Hydrogen Ionophore II mixture A, Selectophore, Fluka).

Analytical Model—Similar to our previous weak acid/base transport model (9, 17), all relevant proton-transfer reactions and diffusion processes were taken into account. Using Fick's 1st and 2nd laws, a set of coupled differential Equations 2 and 3 was written,

$$J_i^{cis}(x) = -D_i\frac{dc_i^{cis}(x)}{dx}, \frac{dJ_i^{cis}(x)}{dx} = R_i(c^{cis}(x)),$$

$$c^{cis} = (c_1^{cis},\ldots,c_8^{cis}), x \text{ in } (0,\delta), i = 1,\ldots,8, \quad \text{(Eq. 2)}$$

$$J_i^{trans}(x) = -D_i\frac{dc_i^{trans}(x)}{dx}, \frac{dJ_i^{trans}(x)}{dx} = R_i(c^{trans}(x))$$

$$c^{trans} = (c_1^{trans},\ldots,c_8^{trans}), x \text{ in } (\delta, 2\delta) \quad \text{(Eq. 3)}$$

where J_i^{cis}, c_i^{cis}, J_i^{trans}, and c_i^{trans} are, respectively, the fluxes and the concentrations of the ith species in the membrane vicinity in the *cis* and *trans* compartments. The index i denotes the following species: $1 = H^+$, $2 = OH^-$, $3 = A^-$, $4 = AH$, $5 = CO_2$, $6 = HCO_3^-$, $7 = CO_3^{2-}$, $8 = H_2O$. A^- and AH are, respectively, deprotonated and protonated buffer molecules. D_i and R_i symbolize the corresponding diffusion coefficients and the specific local rates of expenditure as shown in Equation 4,

$$R_1(c) = (k_{+1}c_8 - k_{-1}c_1c_2) + (k_{-2}c_5 - k_{+2}c_1c_6) + (k_{-3}c_6 - k_{+3}c_1c_7) + (k_{+5}c_4 - k_{-5}c_1c_3)$$

$$R_2(c) = (k_{+1}c_8 - k_{-1}c_1c_2) + (k_{+4}c_6 - k_{-4}c_5c_2)$$

$$R_3(c) = -R_4(c) = (k_{+5}c_4 - k_{-5}c_1c_3)$$

$$R_5(c) = (k_{+2}c_1c_6 - k_{-2}c_5) + (k_{+4}c_6 - k_{-4}c_2c_5)$$

$$R_6(c) = (k_{-2}c_5 - k_{+2}c_1c_6) + (k_{+3}c_1c_7 - k_{-3}c_6) + (k_{-4}c_5c_2 - k_{+4}c_6)$$

$$R_7(c) = (k_{-3}c_6 - k_{+3}c_1c_7)$$

$$R_8(c) = (k_{-1}c_1c_2 - k_{+1}c_8) \quad \text{(Eq. 4)}$$

valid for both $c = c^{cis}$ and $c = c^{trans}$. The notations of kinetic rates and equilibrium constants are depicted in Fig. 1. The corresponding values are listed in Table 1.

At $x = \delta$ the fluxes of all species are required to be equal to zero except for CO_2, where we have Equations 5–7.

$$J_5^{cis} = P_{M,CO_2}(c_5^{cis} - c_5^{trans}) \quad \text{(Eq. 5)}$$

$$J_5^{trans} = -P_{M,CO_2}(c_5^{cis} - c_5^{trans}) \quad \text{(Eq. 6)}$$

with

$$J_{M,CO_2} = |J_5^{cis}| = |J_5^{trans}| \quad \text{(Eq. 7)}$$

If the transmembrane CO_2 flux, $J_{M,CO2}$, is determined by the resistance of near-membrane USLs, the concentration difference c_5^{cis}–c_5^{trans} does not depend on $P_{M,CO2}$. Consequently, only a lower boundary of $P_{M,CO2}$ can be determined from $J_{M,CO2}$ measurements. Above that boundary the analytical model (see Equations 2–7) fit the experimental pH profiles perfectly well for any arbitrary chosen value of $P_{M,CO2}$. To determine the lower boundary, a penalty term for $P_{M,CO2}$ was introduced into the fitting procedure (see "Appendix") that disfavors large $P_{M,CO2}$ values. Finally, the experimental bulk concentrations are used as boundary conditions for the concentrations at $x = 0$ and $x = 2\delta$.

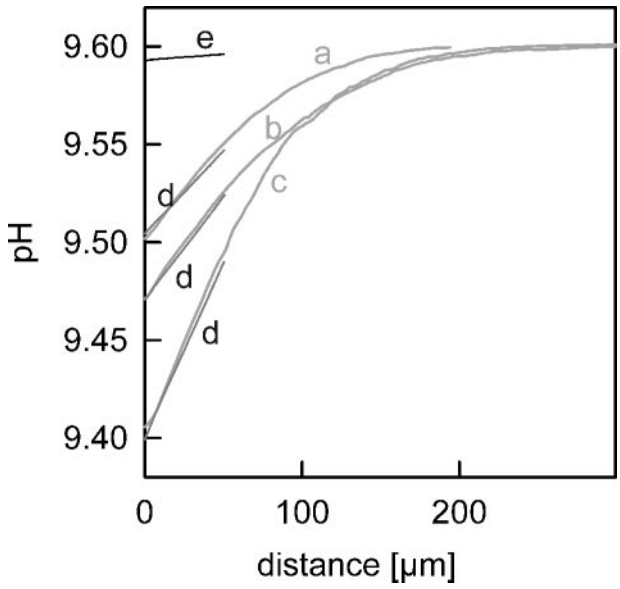

FIGURE 2. **Experimental pH profiles (*gray lines*) in the *trans* USL at pH 9.6.** CO_2 flux from *cis* to *trans* side was induced by the following: *a*, 8 mM HCO_3^- plus 3.2 mM CO_3^{2-}; *b*, 11 mM HCO_3^- plus 4.4 mM CO_3^{2-}; and *c*, 24 mM HCO_3^- plus 9.6 mM CO_3^{2-}. Theoretical pH profiles (*black lines*) were calculated by the analytical model for $P_{M,CO2} = 3.2$ cm/s at the corresponding concentrations (*d*). Decreasing $P_{M,CO2}$ to about 0.016 cm/s (the permeability of ammonia) resulted in profile *e*. Bulk solution contained 30 mM CAPSO, 66 mM NaCl (pH 9.6).

RESULTS

We started our experiments at nonphysiological high pH values because Gutknecht *et al.* (18) reported that for pH > 9 and saturating CA concentrations, USL effects are negligible. To test whether the lipid bilayer constitutes the main diffusion barrier for CO_2 transport under these conditions, we imposed a CO_2 concentration gradient across the membrane and measured resulting pH shifts in the immediate membrane vicinity on the *trans* side (the CO_2 source) at various CO_2 concentrations (Fig. 2). pH was detected by scanning microelectrodes that were moved stepwise in the direction normal to the planar bilayer (17, 19). Increasing concentrations of CO_2 resulted in increasing pH shifts from bulk pH of 9.6. Within a distance of ±50 μm from the membrane surface, the analytical model (Equations 2–7) was fitted to the experimental pH profiles (Fig. 2*d*, *gray lines*) using inverse problem techniques (see "Appendix"). A $P_{M,CO2}$ value of 3.2 cm/s was determined. The system converged with a zero penalty term (see "Experimental Procedures"). Because this term penalizes large $P_{M,CO2}$ values, which may be computed in case flux limitations by USLs, the observation indicated that bilayer resistance to CO_2 flux (J_{CO2}) was not negligible. We subsequently increased the penalty term and found that the lower boundary of $P_{M,CO2}$ that described the measured profile within the experimental error was equal to 1.6 cm/s.

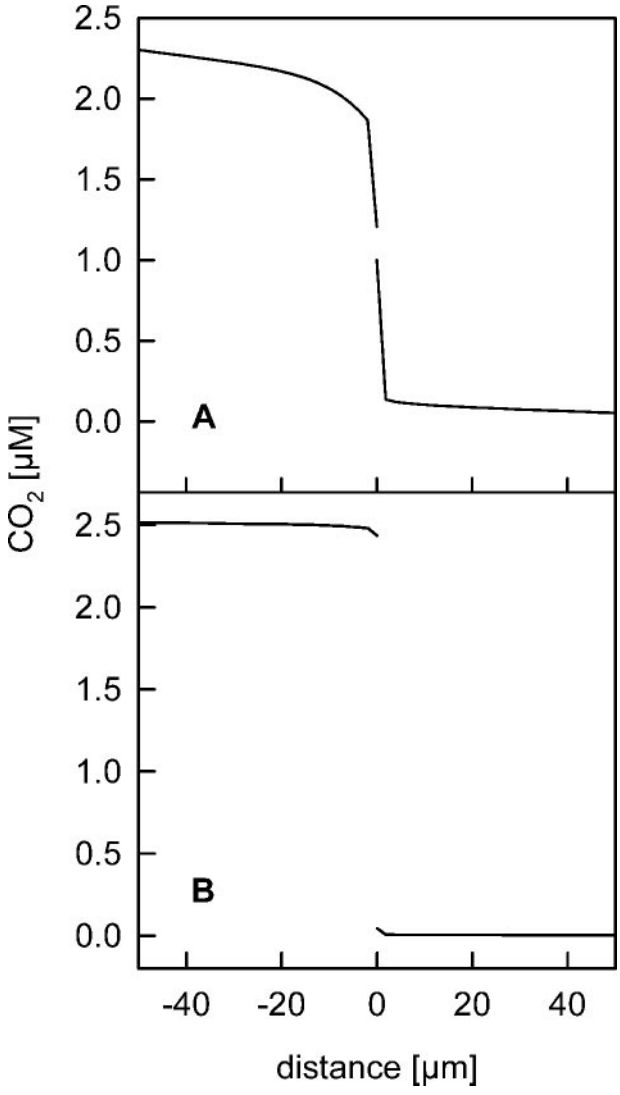

FIGURE 3. **CO_2 concentration as function of the distance to the membrane at pH 9.6.** *A,* profiles are calculated with the fit parameters obtained in Fig. 2. 85% of the resistance to CO_2 flow is because of diffusion through the USL and only 15% is because of permeation through the membrane. Adjacent to the membrane the reaction $CO_2 \Delta H^+ + HCO_3^-$ was not in equilibrium. *B,* calculated CO_2 profiles with the same set of parameters but the membrane permeability of ammonia $P_M = 0.016$ cm/s.

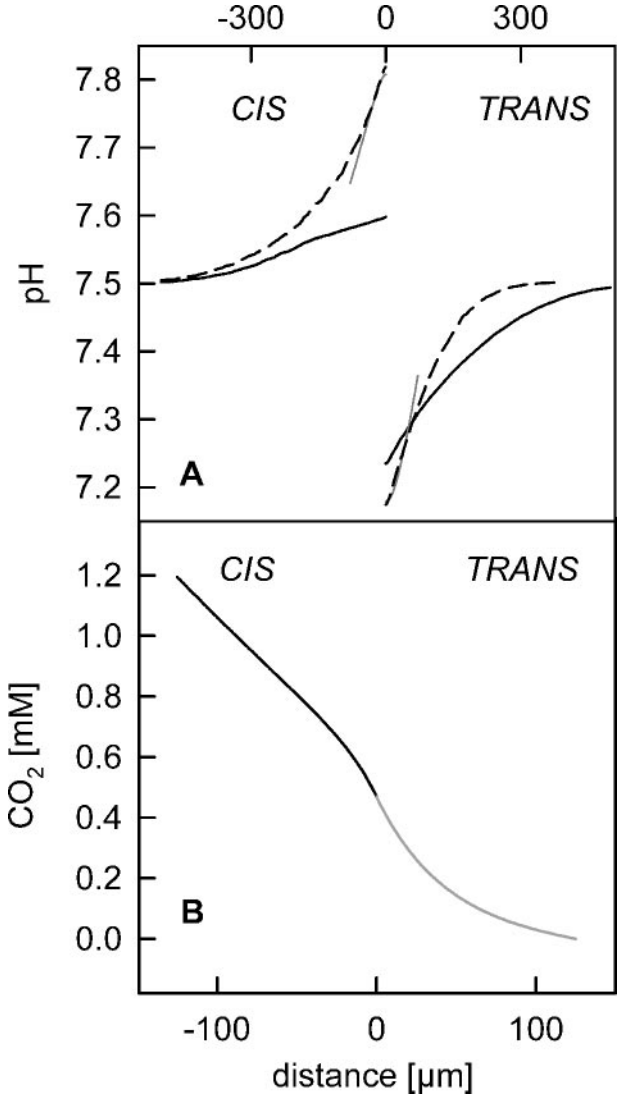

FIGURE 4. **CO_2 concentration and pH shifts adjacent to the membrane at bulk pH 7. 5.** *A,* experimental pH profiles for unilateral (*solid lines*) and bilateral (*dashed lines*) carbonic anhydrase (each 0.5 mg/ml) addition. CO_2 flux was induced by 33 mM HCO_3^- in *cis* side. The bulk solution at both sides of the membrane contained 30 mM HEPES, 66 mM NaCl and was titrated to pH 7.5. The *gray lines* represent theoretical pH profiles for $P_M = 3.2$ cm/s. *B,* CO_2 profiles corresponding to the dashed pH profiles in *A.* Remarkable is the lack of a transmembrane CO_2 concentration gradient.

To demonstrate the validity of Overtone's law, a theoretical profile was calculated assuming that $P_{M,CO2} = P_{M,NH3} = 0.016$ cm/s (*e*). Its discrepancy with our experiment clearly demonstrates that $P_{M,CO2} \gg P_{M,NH3}$.

From the experimental pH profiles (Fig. 2*a*) the corresponding theoretical CO_2 profiles were calculated (Fig. 3). They revealed that most of the resistance (~85%) to CO_2 movement is because of its diffusion through the USL. The observation that membrane permeation is not rate-limiting suggests that the calculated $P_{M,CO2}$ of 3.2 ± 1.6 cm/s is likely to be an underestimation (compare Refs. 9, 17).

It is important to note that within the first few micrometers the protonation-deprotonation reactions of the weak acid are not in equilibrium. Similar reaction layers have previously been observed in the case of acetaldehyde transport at low alcohol dehydrogenase concentrations (20). For H^+, HCO_3^-, and CO_2 to be in equilibrium, the deprotonation rate of HCO_3^- would have to be in the range of 10^{13}–10^{14} M^{-1} s^{-1}, which is clearly nonphysiological. If the permeability value close to that of ammonia is assumed, the steep gradients in the immediate membrane vicinity disappear, and the equilibrium is maintained throughout the USL (Fig. 3*B*).

To study CO_2 permeability under physiological conditions, bulk pH was decreased to 7.5 (Fig. 4*A*). The corresponding spatial CO_2 distribution revealed the lack of a transmembrane CO_2 concentration difference (Fig. 4*B*), indicating that at pH 7.5, CO_2 permeability is completely USL-limited. Removal of CA from the *cis* side of the membrane decreased the flux 2–3-fold. Because of the decrease of the reaction rate, the reaction layer further extended into the solution and was reflected by the pH profile as a deviation from the simple exponential decay. Consequently, the size of the USL, δ, defined in terms of the pH gradient at the membrane water interface increased from

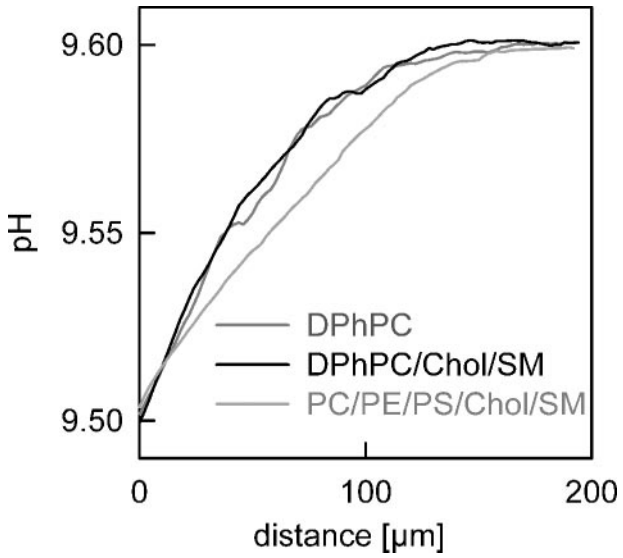

FIGURE 5. **Representative pH profiles for the following: (i) a pure DPhPC bilayer, (ii) a DPhPC bilayer tightened by cholesterol and sphingomyelin, and (iii) a bilayer designed to mimic the red cell plasma membrane.** It was composed of egg phosphatidylcholine (*PC*), egg phosphatidylethanolamine (*PE*), brain phosphatidylserine (*PS*), cholesterol (*Chol*), and egg sphingomyelin. CO_2 flux was induced by 8 mM $NaHCO_3$ and 3.2 mM Na_2CO_3 added in the *cis* side of the membrane. With 1.05 nmol s^{-1} cm^{-2} (i), 1.12 nmol s^{-1} cm^{-2} (ii), and 0.99 nmol s^{-1} cm^{-2} (iii), the proton fluxes did not significantly differ from each other. From 13 runs, mean value and standard deviation were determined as 1.04 ± 0.17 nmol s^{-1} cm^{-2}. For experimental conditions see Fig. 2.

160 μm to more than 500 μm (Fig. 4*A*). In line with a previous report by Gutknecht *et al.* (18), total lack of CA in both compartments resulted in a large decrease of the CO_2 flux and thus in an undetectable small interfacial pH shift (data not shown).

If our conclusion was correct and CO_2 diffusion through the membrane is not rate-limiting, changes of membrane composition are not expected to result in alterations of CO_2 membrane permeability. Thus, in contrast to membrane permeabilities of water (21, 22) and ammonia (2, 9, 23), membrane tightening by cholesterol and SM should not alter the apparent CO_2 permeability of 3.2 cm/s. At least three effects contribute to the reduction in membrane microviscosity (24, 25). (i) Cholesterol increases the packing density of lipids. (ii) Sphingomyelin molecules form strong hydrogen bonds with each other and with cholesterol. (iii) The fully saturated SM lowers the bilayer content of unsaturated fatty acids. In line with our anticipation, we did not observe significant differences in the CO_2 -coupled proton fluxes adjacent to (i) pure DPhPC membranes, (ii) DPhPC membranes tightened by cholesterol and SM, and (iii) bilayers mimicking the composition of red blood cell membranes (Fig. 5). As the presence of cholesterol and SM is associated with both decreased membrane fluidity and decreased membrane diffusion coefficients of water and solutes (23, 26), the CO_2 flux invariability indicates that the lipid bilayer does not act as a barrier to CO_2 diffusion.

Because USL adjacent to biological membranes are about 2 orders of magnitude smaller than those adjacent to planar bilayers, we calculated the contribution a 1-μm-thick USL would make to CO_2 membrane resistance. Solving the inverse

TABLE 1

List of parameters used in our computations

The dissociation constant is expressed as $K = 10^{-pK} = k_d/k_a$. Parameters and parameter ranges, respectively, are taken from Refs. 7, 12, 17, 18, 39.

Parameter	Value
D_1	9.31×10^{-9} (m^2 s^{-1})
D_2	5.26×10^{-9} (m^2 s^{-1})
$D_{3,4}$	5.1×10^{-10} (m^2 s^{-1})
D_5	2.9×10^{-9} (m^2 s^{-1})
$D_{6,7}$	2×10^{-9} (m^2 s^{-1})
D_8	2.5×10^{-9} (m^2 s^{-1})
pK_a	15.74
pK_b	6.1
pK_c	10
k_d	1.26×10^{-8}
pK_e	9.6
k_{-1}	5×10^{11} (m^3 $s^{-1}$$kmol^{-1}$)
k_{+2}	2×10^6–2×10^7 (m^3 $s^{-1}$$kmol^{-1}$)
k_{+3}	1×10^{10}–2×10^{10} (m^3 $s^{-1}$$kmol^{-1}$)
k_{-4}	1×10^8–8.5×10^9 (m^3 $s^{-1}$$kmol^{-1}$)
k_{-5}	1×10^{10}–2×10^{10} (m^3 $s^{-1}$$kmol^{-1}$)

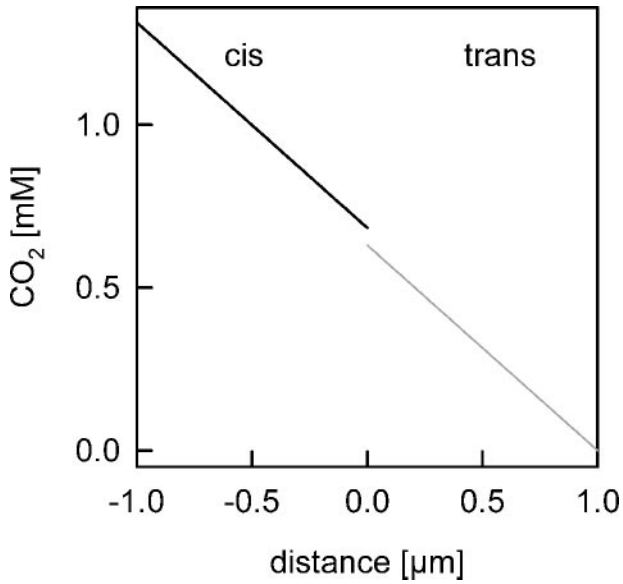

FIGURE 6. **Theoretical CO_2 profiles for USLs that are 1 μm in size.** All model parameters were taken from Fig. 4 (pH 7.5). 95% of the transport resistance was caused by the diffusion through the USL, *i.e.* the membrane did not act as a barrier to CO_2 diffusion. Because the size of the USLs adjacent to cells commonly exceeds 1 μm, transport facilitation by proteins in their plasma membranes is highly unlikely.

problem with all model parameters but δ unaltered (Table 1, pH 7.5), we found that such an USL still imposes ~95% of the total resistance to CO_2 flow (Fig. 6). Because, for example, red blood cells have a USL that exceeds 1 μm in size (27–29), an AQP1-facilitated CO_2 diffusion across red blood cell membranes is extremely unlikely. A meaningful physiological contribution of protein channels to CO_2 transport remains doubtful even if they function in tight epithelial membranes. The prediction was confirmed by studying CO_2 transport through monolayers of AQP1 overexpressing MDCK cells (Fig. 7). Although the presence of AQP1 in both the apical and basolateral membranes (Fig. 7, *A* and *B*) mediated a 3-fold increase in water flux (Fig. 7*C*), the pH profiles measured in the presence of a transepithelial CO_2 gradient (Fig. 7*D*) indicated that the CO_2 fluxes across AQP1 expressing and nonexpressing cells were identical (Fig. 7*D*).

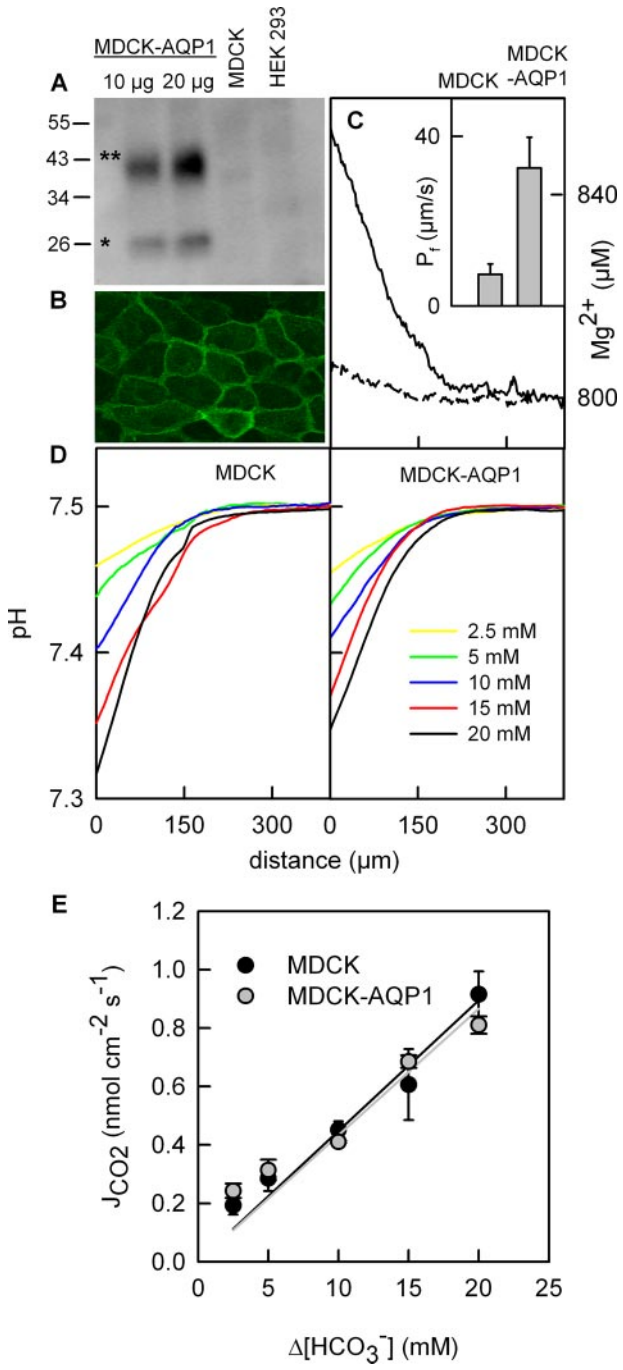

FIGURE 7. **Water and CO_2 transport through monolayers formed by MDCK cells and by AQP1 overexpressing MDCK cells (MDCK-AQP1).** *A,* immunoblot of cell lysates probed with AQP1 antibody. Both nonglycosylated (*) and glycosylated (**) forms of AQP1 were observed (compare also 38). *B,* immunofluorescence of MDCK-AQP1 cells. An antibody against human AQP1 and a FITC-labeled secondary antibody were used. Nontransfected MDCK cells as well as MDCK-AQP1 cells treated solely with FITC-labeled secondary antibody did not show immunofluorescence (data not shown). *C,* water permeability was measured by imposing an osmotic gradient of 380 mM (500 mM sorbitol added) over the epithelial monolayer and detecting the dilution of Mg^{2+} ions close to the basolateral membrane surface with a scanning ion-sensitive microelectrode (*left panel*). Seven independent runs of the experiment ($n = 7$) indicated that AQP1 accounted for 2/3 of the total water flux (*inset*). *D,* representative pH profiles measured in the presence of the indicated HCO_3^- gradients across monolayers formed by MDCK and MDCK-AQP1 cells. The slope at the membrane water interface is crucial for flux calculation. Differences in the profile course between MDCK and MDCK-AQP1 cells are solely because of variations in the stirring conditions. *E,* CO_2 fluxes across AQP1 expressing and nonexpressing cells were identical ($n = 10$).

DISCUSSION

As predicted by Overtone's rule, the lipid matrix of biological membranes does not represent a barrier to CO_2 transport. Measurements of pH shifts in the immediate vicinity of planar bilayers and epithelial monolayers demonstrate that near-membrane USLs generate the main resistance to CO_2 flow. Model simulations confirm that the result is valid for USLs less than 1-μm-thick. Because membrane tightening by cholesterol and SM does not reduce membrane CO_2 permeability below 3.2 cm/s, facilitation of CO_2 membrane transport by proteinaceous molecules is virtually impossible. Here, CO_2 transport differs fundamentally from ammonia and water transport, which, in the absence of specific membrane channels, exhibit permeabilities that are orders of magnitude smaller (2, 9, 22).

The lack of a facilitating effect of aquaporins on CO_2 transport has been demonstrated before using knock-out mice (11). However, the conclusion of this study was debated (3, 5, 30) because the authors used kinetic measurements that were hampered by USL effects (11). Moreover, the apparent membrane permeability of 0.011 cm/s (11) would have been very compatible with the idea of a protein-mediated CO_2 transport (31–35). The widely used rapid mixing experiments were recently supplemented by a mass spectrometry approach, which was claimed to be less sensitive to USL effects because of a hypothetical store of bicarbonate near the membrane surface (3, 5). Our steady-state pH measurements in the immediate membrane vicinity have now shown that this assumption was not correct. In addition, the unilateral CA activity as used by Endeward *et al.* (3, 5) and Vandegriff and Olson (29) resulted in the appearance of an extended reaction layer that prevented correct measurements of CO_2 membrane permeability (Fig. 4). Even if the authors were able to add CA to both sides of their membranes, the applicability of a method would be questionable, which according to the approximation by Endeward *et al.* (3, 5) is limited to permeability values well below 1 cm/s.

Regulation of CO_2 transport by proteins is not necessarily limited to the tuning of CA activity. Instead of facilitating CO_2 transport, proteins may act to lower CO_2 permeability. Such an assumption would explain how gastric gland cells exclude CO_2 to protect themselves from the rough conditions in the gastric gland lumen (37). Studies are underway to clarify the barrier function of peripheral proteins.

Acknowledgments—We thank Peter Deen and Hans Oberleitner for providing the MDCK-AQP1 cells and the MDCK cells, respectively.

REFERENCES

1. Khademi, S., O'Connell, J., III, Remis, J., Robles-Colmenares, Y., Miercke, L. J., and Stroud, R. M. (2004) *Science* **305,** 1587–1594
2. Saparov, S. M., Liu, K., Agre, P., and Pohl, P. (2007) *J. Biol. Chem.* **282,** 5296–5301
3. Endeward, V., Musa-Aziz, R., Cooper, G. J., Chen, L. M., Pelletier, M. F., Virkki, L. V., Supuran, C. T., King, L. S., Boron, W. F., and Gros, G. (2006) *FASEB J.* **20,** 1974–1981
4. Uehlein, N., Lovisolo, C., Siefritz, F., and Kaldenhoff, R. (2003) *Nature* **425,** 734–737
5. Endeward, V., Cartron, J. P., Ripoche, P., and Gros, G. (2007) *FASEB J.* **22,** 1–11
6. Walter, A., and Gutknecht, J. (1986) *J. Membr. Biol.* **90,** 207–217

7. Saparov, S. M., Antonenko, Y. N., and Pohl, P. (2006) *Biophys. J.* **90,** L86–L88
8. Simon, S. A., and Gutknecht, J. (1980) *Biochim. Biophys. Acta* **596,** 352–358
9. Antonenko, Y. N., Pohl, P., and Denisov, G. A. (1997) *Biophys. J.* **72,** 2187–2195
10. Barry, P. H., and Diamond, J. M. (1984) *Physiol. Rev.* **64,** 763–872
11. Yang, B. X., Fukuda, N., van Hoek, A., Matthay, M. A., Ma, T. H., and Verkman, A. S. (2000) *J. Biol. Chem.* **275,** 2686–2692
12. Hub, J. S., and de Groot, B. L. (2006) *Biophys. J.* **91,** 842–848
13. Wang, Y., Cohen, J., Boron, W. F., Schulten, K., and Tajkhorshid, E. (2007) *J. Struct. Biol.* **157,** 534–544
14. Devaux, P. F., and Seigneuret, M. (1985) *Biochim. Biophys. Acta* **822,** 63–125
15. Mueller, P., Rudin, D. O., Tien, H. T., and Wescott, W. C. (1963) *J. Phys. Chem.* **67,** 534–535
16. Deen, P. M., Nielsen, S., Bindels, R. J., and van Os, C. H. (1997) *Pfluegers Arch.* **433,** 780–787
17. Antonenko, Y. N., Denisov, G. A., and Pohl, P. (1993) *Biophys. J.* **64,** 1701–1710
18. Gutknecht, J., Bisson, M. A., and Tosteson, D. C. (1977) *J. Gen. Physiol.* **69,** 779–794
19. Pohl, P., Antonenko, Y. N., and Rosenfeld, E. H. (1993) *Biochim. Biophys. Acta* **1152,** 155–160
20. Antonenko, Y. N., Pohl, P., and Rosenfeld, E. H. (1996) *Arch. Biochem. Biophys.* **333,** 225–232
21. Hill, W. G., and Zeidel, M. L. (2000) *J. Biol. Chem.* **275,** 30176–30185
22. Krylov, A. V., Pohl, P., Zeidel, M. L., and Hill, W. G. (2001) *J. Gen. Physiol.* **118,** 333–340
23. Lande, M. B., Donovan, J. M., and Zeidel, M. L. (1995) *J. Gen. Physiol.* **106,** 67–84
24. Smaby, J. M., Brockman, H. L., and Brown, R. E. (1994) *Biochemistry* **33,** 9135–9142
25. Huster, D., Arnold, K., and Gawrisch, K. (1998) *Biochemistry* **37,** 17299–17308
26. Finkelstein, A., Zimmerberg, J., and Cohen, F. S. (1986) *Annu. Rev. Physiol.* **48,** 163–174
27. Huxley, V. H., and Kutchai, H. (1981) *J. Physiol.* (*Lond.*) **316,** 75–83
28. Coin, J. T., and Olson, J. S. (1979) *J. Biol. Chem.* **254,** 1178–1190
29. Vandegriff, K. D., and Olson, J. S. (1984) *J. Biol. Chem.* **259,** 12609–12618
30. Cooper, G. J., Zhou, Y., Bouyer, P., Grichtchenko, I. I., and Boron, W. F. (2002) *J. Physiol.* (*Lond.*) **542,** 17–29
31. Forster, R. E., Gros, G., Lin, L., Ono, Y., and Wunder, M. (1998) *Proc. Natl. Acad. Sci. U. S. A.* **95,** 15815–15820
32. Prasad, G. V., Coury, L. A., Finn, F., and Zeidel, M. L. (1998) *J. Biol. Chem.* **273,** 33123–33126
33. Blank, M. E., and Ehmke, H. (2003) *J. Physiol.* (*Lond.*) **550,** 419–429
34. Soupene, E., King, N., Feild, E., Liu, P., Niyogi, K. K., Huang, C. H., and Kustu, S. (2002) *Proc. Natl. Acad. Sci. U. S. A.* **99,** 7769–7773
35. Cooper, G. J., and Boron, W. F. (1998) *Am. J. Physiol.* **275,** C1481–C1486
36. Engl, H. W., and Kügler, P. (2005) in *Series Mathematics in Industry* (Capasso, V., and Periaux, J., eds) pp. 3–47, Springer-Verlag, Heidelberg
37. Waisbren, S. J., Geibel, J. P., Modlin, I. M., and Boron, W. F. (1994) *Nature* **368,** 332–335
38. Preston, G. M., Jung, J. S., Guggino, W. B., and Agre, P. (1993) *J. Biol. Chem.* **268,** 17–20
39. Gutman, M., and Nachliel, E. (1995) *Biochim. Biophys. Acta* **1231,** 123–138
40. Deuflhard, P. (2004) in *Springer Series in Computational Mathematics* (Bank, R. E., Graham, R., Stoer, J., Varga, R. S., and Yserentant, H., eds) Vol. 35, Springer-Verlag, Heidelberg

APPENDIX

Solving the Analytical Model—Given values for the permeability P_M, the kinetic rates and equilibrium constants, and the boundary conditions, the experimentally observed pH profile can be simulated using the analytical model. For that purpose, one solves the nonlinear system of the differential Equations 2 and 3 for all concentrations, $C = (c^{cis}, c^{trans})$, which then allows us to calculate the pH profile as $-\log(c_1^{trans}(X))/\log(10)$ with X in $(\delta, 2\delta)$. To calculate the solution C of the nonlinear system (Equations 2 and 3) in the following, abbreviated as $U(C) = 0$, typically Newton-type methods (see 40) are chosen. Given a solution guess C_{-k}, the central idea is to solve a linearized problem, which in its simplest form reads as shown in Equation 8,

$$U'(C_{-k})\mathsf{H} = -U(C_{-k}) \quad \text{(Eq. 8)}$$

and to build a new solution guess via Equation 9,

$$C_{-k+1} = C_{-k} + \lambda \mathsf{H}_{-k} \quad \text{(Eq. 9)}$$

This procedure is iterated, with the damping factor λ possibly varying from step to step, until a suitably accurate solution is obtained. Of course, for the numerical realization of the iteration procedure, the differential Equations 2 and 3 have to be discretized and the various concentration values at the grid points of the mesh laid over $(0,\delta)$ and $(\delta,2\delta)$ become the unknowns of the system. With respect to the linearized problem, this amounts to solving a high dimensional system of linear equations with a sparse matrix $U'(C_{-k})$, whereas the iteration then takes places in a vector space. All numerical solutions of Equations 2 and 3 used in this paper have been obtained by use of the finite element software package COMSOL Multiphysics (Göttingen, Germany).

Solving the Inverse Problem for P_M—The experimental pH profile data were used to determine the permeability P_M while allowing the other uncertain model parameters $k_{+2}, k_{+3}, k_{-4}, k_{-5}$ of Equations 2 and 3 to vary within the bounds given by Table 1. Using the notation $q = (P_M, k_{+2}, k_{+3}, k_{-4}, k_{-5})$, the inverse problem can be formulated as nonlinear operator Equation 10,

$$F(q) = y \quad \text{(Eq. 10)}$$

where F is the so-called parameter-to-output map. Assuming that for any vector q out of an admissible set Q the direct problem $U(C) = 0$ admits a unique solution $C(x;q)$, the operator F is defined as shown in Equation 11,

$$F{:}q \rightarrow -\log(c_1^{trans}(x;q))/\log(10) \quad \text{(Eq. 11)}$$

Note that F is only implicitly defined, and its evaluation requires solving $U(C) = 0$ for $C(x;q)$ and calculating the simulated pH profile. Because solvability of the inverse problem in the strict sense cannot be guaranteed because of modeling and measurement errors, the inverse problem is approached via minimization of the Tikhonov type functional as shown in Equation 12,

$$J(q) := \|y - F(q)\|^2 = \int_{\delta}^{2\delta} (y(x) - (-\log(c_1^r(x,q))/\log(10)))^2 dx + \alpha\, \text{penalty}(q) \rightarrow \min q \in Q \quad \text{(Eq. 12)}$$

Such parameter identification problems typically are ill-posed in the sense that the solution q sought for does not depend continuously on the data, *i.e.* small deviations in y can lead to

large deviations in the solution. These instabilities can be overcome by the use of regularization methods (see Ref. 36 for an overview). In the popular Tikhonov type regularization methods, the stabilization effect is because of an additional penalty term on the parameter q. Because of the low dimensionality of the parameter vector q in our application, the bounds on k_{+2}, k_{+3}, k_{-4}, k_{-5} according to Table 1 and the constraints 0.001 cm/s $\leq P_M \leq$ 100 cm/s, the ill-posed effects are rather negligible. Hence, we only use penalty $(q) = {P_M}^{0.1}$ in order to look for a small value of the permeability that still allows us to explain our experimental observations.

For the numerical realization the integral was approximated by a trapezoidal rule, whereas the objective function J was minimized using a combination of the MATLAB (Mathworks, Natick, MA) routines ga, patternsearch, and fminsearch of the Genetic Algorithm and Direct Search Toolbox. Although conceptionally different, all of these derivative free optimization routines approach the minimizer in an iterative procedure defining a minimizing sequence q^k. Note that for each iterate q^k the evaluation of the objective J requires solving the direct problem $U(C) = 0$ for $C(x;q^k)$. To reduce the chance of only obtaining a local minimizer, the optimization problem has been solved independently several times.

We actually recorded a sequence of pH profiles, *i.e.* $y^j(x)$ for x in $(\delta, 2\delta)$, $j = 1,2,3$, as a result to considerations of three different boundary concentrations $c_{6,j}^{cis}(0)$ of HCO_3^- on the *cis* side. In the mathematical formulation of the inverse problem, this simply is taken into account via the sequence of nonlinear problems shown in Equation 13.

$$F_j(q) = y^j; j = 1,2,3 \qquad \text{(Eq. 13)}$$

where F_j denotes the parameter-to-output map defined via $U(C) = 0$ with the choice $c_6^{cis}(0) = c_{6,j}^{trans}(0)$. As objective functional we then considered is shown in Equation 14.

$$J(q) := \sum_{j=1}^{3} w_j \|y^j - F_j(q)\|^2 + \alpha P_M^{0,1} \rightarrow \min q \in Q \qquad \text{(Eq. 14)}$$

where the weights w_j and α have been chosen according to $w_j = 1/\|y^j\|^2$ and $\alpha = 0.0001$.